Implementation and experimental validation of a modeling tool for humid air turbine saturators

Francesco Caratozzolo, Alberto Traverso, Aristide F. Massardo

▶ To cite this version:

HAL Id: hal-00789876
https://hal.science/hal-00789876

Accepted Manuscript

Title: Implementation and experimental validation of a modeling tool for humid air turbine saturators

Authors: Francesco Caratozzolo, Alberto Traverso, Aristide F. Massardo
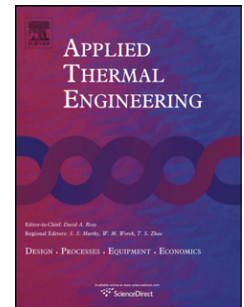
Please cite this article as: F. Caratozzolo, A. Traverso, A.F. Massardo. Implementation and experimental validation of a modeling tool for humid air turbine saturators, Applied Thermal Engineering (2011), doi: 10.1016/j.applthermaleng.2011.07.022

IMPLEMENTATION AND EXPERIMENTAL VALIDATION OF A MODELING TOOL FOR HUMID AIR TURBINE SATURATORS

Francesco Caratozzolo **Alberto Traverso** **Aristide F. Massardo**

francesco.caratozzolo@unige.it alberto.traverso@unige.it massardo@unige.it

Thermochemical Power Group (TPG) – DIMSET, Università di Genova, Genova, Italy

ABSTRACT

This work presents the re-engineering of the TRANSAT 1.0 code which was developed to perform off-design and transient condition analysis of Saturators and Direct Contact Heat Exchangers. This model, now available in the 2.0 release, was originally implemented in FORTRAN language, has been updated to C language, fully coded into MATLAB/Simulink® environment and validated using the extensive set of data available from the MOSAT project, carried out by the Thermochemical Power Group of the University of Genoa. The rig consists of a fully instrumented modular vertical saturator, which is controlled and monitored with a LABVIEW® computer interface. The simulation software showed fair stability in computation and in response to step variation of the main parameters driving the thermodynamic evolution of the air and water flows. Overall the model proved to be reliable and accurate for energy systems simulations.

NOMENCLATURE

A	section area [m^2]
a	liquid/gas interface area [m^2/m^3]
b	parameter for eq. (20) [J/(kg•m•K^2)]
c_p	constant pressure specific heat [J/(kg•K)]
c_v	constant volume specific heat [J/(kg•K)]
dz	infinitesimal saturator cell height [m]
$d\dot{m}_c$	condensate mass flow [kg/s]
h	enthalpy [J/(kg•K)], convective heat transfer coefficient [W/m^{2}K]
h'	dry enthalpy [J/kg$_{da}$]
h_{fg}	latent heat of vaporization [J/(kg•K)]
HAT	Humid Air Turbine
k	conductive heat transfer coefficient [W/m•K]

k_x	mass transfer coefficient [kmol/s m^2]
in	inlet
L	length [m]
M	mass [kg]
$\dot{m}$	mass flow [kg/s]
$MOSAT$	MOdularSATurator
out	outlet
os	over-saturation
p	pressure [Pa]
q	heat flux [kW]
r	radius [m]
R	thermal resistance [K/W]
t	time [s]
T	temperature [K]
th	thickness [m]
u	velocity [m/s]
U	heat transfer coefficient [W/(m^2•K)]
V	volume [m^3]
x	mass fraction
$\tilde{x}$	mole fraction [mol]
Y	absolute humidity [kg$_v$/kg$_{da}$]
z	compressibility factor

Greek letters

ρ	density [kg/m^3]
σ	thermal conductivity [W/(m•K)]
$\varDelta$	difference (delta)

Subscripts

c	condensate
e	external
eff	effective
da	dry air
g	gas phase
i	interface, internal
l	liquid phase
m	metal
mix	mixture
n	n-th component

s	saturation
t	total
v	water vapor
w	water
∞	infinite
*	corrected

Superscripts

c	convective
k	conductive
m	parameter for eq. (20)
'	dry

18

1. INTRODUCTION

19

20   The diffusion of small gas turbines for distributed power production led designers to study ways of increasing the efficiency and

21   specific work of the recuperated Brayton cycle without increasing system complexity and related costs.

22   The Humid Air Turbine (HAT) technology [1] can greatly enhance gas turbine performance in terms of increased efficiency and

23   specific work output. Compared to other mixed air/steam cycles, the HAT configuration introduces the "saturator" into the plant

24   layout: this device carries out a direct contact exchange of heat and mass between two counter-flowing currents of liquid water and

25   compressed air. In this framework a saturator for HAT cycles proved to be a relatively simple component for integration into a simple

26   gas turbine [2][3][4].

27   A detailed and accurate modeling of the saturator is necessary for the complete understanding of both the component behavior and

28   its integration into the whole gas turbine cycle. If the off-design performance modeling is useful for assessing the part-load

29   performance of the plant, the transient analysis is very helpful for studying the dynamic behavior of the plant and for developing

30   proper control systems [3] to follow the loads or to compensate for different ambient conditions.

31   The saturator on-design and off-design models have already been presented by Parente et al. in [5] and a first original transient

32   model, TRANSAT 1.0, has been developed Cevasco et al. in [6]. The availability of new experimental data was the motivation for the

33   review of the model, as described in this paper. Release 2.0 of TRANSAT model is now available not only for theoretical

34   investigations but also for commercial design and analysis.

35   The TRANSAT 2.0 code has already been used for the design and the characterization of a direct contact heat exchanger for

36   application in a zero emission power plant in the Veneto region (Italy). The thermodynamic characterization of a direct contact

37   condenser for ENEL, the major Italian utility, in order to build a H_2-fed combined cycle, with water recovery from the exhaust, was

38   carried out experimentally and the TRANSAT 2.0 code was used to verify the accuracy of experimental data and to accomplish

39   detailed performance analysis. The direct contact heat exchanger, derived from saturators technology, can be used as a condenser [7]of

40   the steam contained in the gas flow at turbine outlet.

41

2. TRANSAT 2.0 CODE OVERVIEW

42

43   TRANSAT 1.0 was presented in [6].

44 The TRANSAT 2.0 code aims at transient and off-design analysis of saturators, humidification towers and direct contact heat

45 exchangers equipped with structured packing.

46 Now TRANSAT 2.0 is entirely coded in C programming language and embedded in MATLAB/Simulink® environment; a

47 Graphic User Interface simplifies data input and outputs analysis (Figure 1).

48 A full re-engineering of code architecture was carried out as a preliminary operation for the present work. The code has been

49 translated from FORTRAN language to C language allowing easier and more flexible integration in MATLAB environment. This

50 recoding led to significant improvements of code computational performance without loss of accuracy. The simulation is now

51 significantly faster than 1.0 with improved stability, allowing the reduction of the number of computation cells and increase of

52 integration time step (e.g. on the same case study, the number of computation cells was decreased from 100 to 50 and the integration

53 time step was increased from 0.01 to 0.1).

54

55 **3. SATURATOR TRANSIENT MODEL**

56 The transient model adopted in the TRANSAT 2.0 code is an evolution of the model employed in the steady-state SAT code [5].

57 Referring to the original set of 1-D equations used in the SAT code, an additional term for energy storage was introduced to

58 account for the unsteadiness of the system. The system is considered to be adiabatic, thus no thermal loss is included in the model. The

59 impact of this assumption is discussed in the paragraph about validation. The droplet size is assumed to be large enough to neglect the

60 influence of surface tension. The radiation is neglected due to moderate temperatures.

61 The code is able to handle a wide range of gas species by setting the proper composition, 28 components are available to specify

62 the mixture. The liquid phase can be only water. Considering the saturator discretization in N cells, such as the one represented in

63 Figure 2, the balance equations can now be written as follows:

64 Enthalpy balance – Liquid side

$$\dot{m}_{l,j+1} \cdot h_{l,j+1} - \dot{m}_{l,j} \cdot h_{l,j} + d\dot{m}_c \cdot h_l(\overline{T}_g) - [(d\dot{m}]_l + d\dot{m}_c) \cdot h_l(\overline{T}_i) - U_l^c \cdot (\overline{T}_l - \overline{T}_i) \cdot a \cdot dz = \bar{c}_{v,l} \cdot M_{l,j} \cdot {\partial T_{l,j}}/{\partial t} \tag{1}$$

65 Enthalpy balance – Gas side

$$\dot{m}_{g,j} \cdot h_{g,j} - \dot{m}_{g,j+1} \cdot h_{g,j+1} + U_g^c \cdot (\overline{T}_i - \overline{T}_g) \cdot a \cdot dz + [(d\dot{m}]_l + d\dot{m}_c) \cdot h_v(\overline{T}_i) - d\dot{m}_c \cdot h_l(\overline{T}_g) = \bar{c}_{v,g} \cdot M_{g,j+1} \cdot {\partial T_{g,j+1}}/{\partial t} \tag{2}$$

66 Global enthalpy balance

67 The global enthalpy balance in equation (3) can be obtained considering equation (4) that is equivalent to assume no thermal losses
68 and no thermal capacitance at the interface.
69

$$\dot{m}_{l,j+1} \cdot h_{l,j+1} - \dot{m}_{l,j} \cdot h_{l,j} + \dot{m}_{g,j} \cdot h_{g,j} - \dot{m}_{g,j+1} \cdot h_{g,j+1} = \bar{c}_{v,l} \cdot M_{l,j} \cdot {\partial T_{l,j}}/{\partial t} + \bar{c}_{v,g} \cdot M_{g,j+1} \cdot {\partial T_{g,j+1}}/{\partial t} \tag{3}$$

$$\left(U_l^c \cdot (\overline{T}_l - \overline{T}_i) - U_g^c \cdot (\overline{T}_i - \overline{T}_g)\right) \cdot a \cdot dz + [(d\dot{m}]_l + d\dot{m}_c) \cdot \left(h_l(\overline{T}_i) - h_v(\overline{T}_i)\right) = 0 \tag{4}$$

70   In the previous equations all the terms were evaluated at a generic time instant n. The subscripts j and j+1 refer to the section

71   where the respective term is being evaluated, while the symbol "‾" indicates that the respective term is the mean cell value. The

72   unsteady terms in the continuity and momentum equations were ignored.

73   The liquid and gas mass in equations (1-3) can be evaluated as follows:

$$M_{g,j+1} = V_g \cdot \bar{\rho}_g = dz \cdot \frac{\dot{m}_g + d\dot{m}_l + d\dot{m}_c}{\bar{\bar{u}}_{g,eff}} \tag{5}$$

$$M_{l,j} = V_l \cdot \bar{\rho}_l = dz \cdot \frac{\dot{m}_l}{\bar{\bar{u}}_{l,eff}} \tag{6}$$

74

75   The total liquid mass flow that evaporates across the cell is determined by:

$$d\dot{m}_c = d\dot{m}_l + d\dot{m}_c = M_w \cdot k_x \cdot \ln\left(\frac{1 - \bar{\bar{x}}_{w,g}}{1 - \bar{\bar{x}}_{w,i}}\right) \cdot a \cdot dz \tag{7}$$

76

77   The term dm_l accounts for the actual liquid evaporation, while the term dm_c accounts for droplet condensation whenever the gas

78   temperature is below the corresponding vapor saturation temperature: it is assumed that the droplet condensate remixes with the liquid

79   phase at the current gas temperature, otherwise this term is set to zero.

80   In the current model version, with respect to TRANSAT 1.0 implementation, the following assumption is made for the equations

81   (1-10):

$$T_i = T_l \tag{8}$$

82

83   The interface temperature and the liquid temperature are supposed to be close and here they are assumed to be equal for

84   simplicity, the same hypothesis was made in [3].

85   Introducing the specific heat in equations (1-2), and assuming (n+1) as the reference instant, the previous relationships can be

86   written as:

$$-\left(\dot{m}_{l,j+i} \cdot \bar{c}_{p,l} + d\dot{m}_l \cdot \bar{c}_{p,li}\right) \cdot T_{l,j+1}^{n+1} + \left(\dot{m}_{l,j} \cdot \bar{c}_{p,l} - \bar{c}_{v,l} \cdot M_{l,j}/{\Delta t}\right) \cdot T_{l,j}^{n+1} \tag{9}$$

$$= \left(\bar{c}_{v,l} \cdot M_{l,j}/{\Delta t}\right) \cdot T_{l,j}^{n} + d\dot{m}_c \cdot \left(h_l(\bar{T}_g) - h_l(\bar{T}_i)\right) - U_l^c \cdot (\bar{T}_l - \bar{T}_i) \cdot a \cdot dz - d\dot{m}_l \cdot \bar{c}_{p,li} \cdot \bar{T}_i$$

$$-\left(\dot{m}_g \cdot \bar{c}_{p,as} + \dot{m}_{v,j} \cdot \bar{c}_{p,v}\right) \cdot T_{g,j}^{n+1} + \left(\dot{m}_g \cdot \bar{c}_{p,as} + \dot{m}_{v,j+1} \cdot \bar{c}_{p,v} + d\dot{m}_l \cdot \bar{c}_{p,v} + \bar{c}_{v,g} \cdot M_{g,j+1}/{\Delta t}\right) \cdot T_{g,j+1}^{n+1} \tag{10}$$

$$= \left(\bar{c}_{v,g} \cdot M_{g,j+1}/{\Delta t}\right) \cdot T_{g,j+1}^{n} + d\dot{m}_c \cdot \left(h_v(\bar{T}_i) - h_l(\bar{T}_g)\right) - U_g^c \cdot (\bar{T}_i - \bar{T}_g) \cdot a \cdot dz - d\dot{m}_l \cdot \bar{c}_{p,vi} \cdot \bar{T}_i$$

87   In (9) and (10) it is assumed that all the mean values are calculated at the time instant n. The terms $\overline{c}_{p,li}$ and $\overline{c}_{p,vi}$ are the mean

88 interface specific heat for the liquid and vapor phases, respectively, while the terms $\overline{c}_{p,as}$ and $\overline{c}_{p,v}$ are the mean dry air and vapor

89 specific heats.

90   Knowing the system properties at the instant *n*, the liquid and gas temperatures at the sections *j* and *j+1*, for the instant *(n+1)*, can

91 be determined with equations (9) and (10), respectively. The numerical solution scheme is thus implicit in the gas and water

92 temperatures.

93   The water mass fraction can be written as:

$$x_{w,j+1} = \frac{\frac{d\dot{m}_t}{\dot{m}_g} + \frac{x_{w,j}}{1 - x_{w,j}}}{1 + \frac{d\dot{m}_t}{\dot{m}_g} + \frac{x_{w,j}}{1 - x_{w,j}}} \tag{11}$$

94

95 where $d\dot{m}_t$ can be determined using equation (7).

96   The maximum liquid mass flow that can evaporate is determined by (12):

$$d\dot{m}_l = \left[Y_s \left(T_{g,j+1}^n, p_{g,j+1}^n \right) - Y \left(T_{g,j}^n, p_{g,j}^n \right) \right] \tag{12}$$

97

98   Knowing the liquid mass fraction at saturation conditions for section *(j+1)* at the gas temperature $T_{g,j+1}$, it is possible to

99 compare this with the value from (11). In the event that the actual vapor mass fraction is lower than the saturation value,

100 $d\dot{m}_l = d\dot{m}_t$ and $d\dot{m}_c = 0$. Otherwise part of the evaporated water will re-condense: $d\dot{m}_c$ can be determined with (7),

101 considering the saturation condition at the cell outlet.

102   The heat and mass transfer coefficient are evaluated for each cell using the Bravo, Rocha and Fair correlations for structured

103 packing [8] and Ackerman's factor is used [5][9].

104   In the TRANSAT model the thermal capacity of the packing and the pipes metal is not considered, this is a relevant simplification

105 for the transient behavior analysis. In this respect, when time-dependant behavior of the specific case is largely dominated by packing

106 and/or vessel thermal capacitance, the numerical scheme can be regarded as a "time marching" solution towards steady-state.

107   Two humid air models are available: Hyland & Wexler model [10][11] and Mollier model (see [5], paragraph 3).

108

109 **4. MOSAT TEST RIG LAYOUT**

110   The purpose of "MOSAT project" [12] was to build a test rig able to collect a wide set of experimental data.

111   The plant was built using off-the-shelf components, except for the modular saturation tower vessel. The core of the rig consists of

112 the saturation tower. Structured internal packing, Figure 3, is used because it is attractive for power generation plants due to the

113 relatively small pressure drop along the saturator axis (which applies to the air in a gas turbine cycle moving from the compressor to

114 the expander). In this way the internal geometry, which is relevant to the design phase of the tower and to the validation of simulation

115 models, is precisely parameterized.

116   The test tower is composed of four flanged pipes, and top and bottom structures. A maximum of 8 packing modules, each of 200

117   mm length and 80 mm diameter, can be placed within the tower.

118   The top of the saturator contains the water injectors and the outlet pipe for humid air.

119   The experiments were carried out using water and atmospheric air. A brief discussion on the uncertainty of the experimental

120   results is given in Appendix A.

121   **5. VALIDATION**

122   The validation of TRANSAT 2.0 code using the Simulink environment proved the stability and accuracy of the model according

123   to the underlying hypothesis.

124   Regarding the large set of experimental data produced by the MOSAT test campaign [12] the validation carried out considered

125   just a selected sample of test cases, reported in Table 1.

126   Six calculations with different boundary conditions were carried out in order to cover a wide operating field.

127   Each test case is characterized by a set of input parameters:

128

129   • Gas inlet temperature ($T_{g_{in}}$)

130   • Liquid water inlet temperature ($T_{l_{in}}$)

131   • Operating pressure of the vessel (p)

132   • Gas mass flow rate ($\dot{m}_{g_{in}}$)

133   • Liquid water mass flow rate ($\dot{m}_{l_{in}}$)

134

135   An important control parameter is the Liquid to Gas Ratio (13):

$$L/G = \frac{\dot{m}_{l_{in}}}{\dot{m}_{g_{in}}} \tag{13}$$

136
137   such a parameter dominates the thermodynamic evolution in the saturation tower: when L/G increases, the gas outlet absolute

138   humidity increases. However, for high values of packing height the effect is less significant.

139   The monitored parameters for data analysis and post processing are:

140

141   • Gas outlet temperature ($T_{g_{out}}$)

142   • Liquid water outlet temperature ($T_{l_{out}}$)

143   • Outlet gas mass flow rate ($\dot{m}_{g_{out}}$)

144   • Outlet liquid water mass flow rate ($\dot{m}_{l_{out}}$)

145   • Evaporated water mass flow ($d\dot{m}_{l}$)

146

147   To check the model theoretical validity, a steady state enthalpy balance is considered (14):

$$[(\dot{m}_l + d\dot{m}_l) \cdot (h_l + dh_l) + \dot{m}_g' \cdot h_g' = \dot{m}_l \cdot h_l + \dot{m}_g' \cdot (h_g' + dh_g') \tag{14}$$

148

149   Eq. 13 can show macroscopic errors in model theory or settings. The error weighted over the gas enthalpy drop is a convenient

150 parameter to estimate the accuracy of the overall enthalpy balance.

151   In order to handle mass flows in the order of 0.1 g/s a geometric similitude was used. The effective contact area per unit of mass

152 flow rate was not changed but the gas and water mass flow rates were increased by a factor of 10. The flow velocity was maintained

153 equal to the actual velocity corresponding to the actual mass flow: so an increased diameter was introduced following the relation in

154 equation (15).

$$d^2_{reduced} = d^2_{actual} \cdot \frac{\dot{m}_{reduced}}{\dot{m}_{actual}} \tag{15}$$

155

156 where *reduced* indicates the corrected inputs introduced in the code and *actual* indicates the real inputs from Table 1.

157   Table 1 shows the experimental data from the MOSAT project used as input values for TRANSAT 2.0 steady state validation.

158   In Table 2 the output results obtained from TRANSAT 2.0 simulations are reported.

159   In Table 3 the absolute differences between experimental data and simulated results are shown. In general, it can be observed that

160 the gas outlet temperature is accurately predicted, whereas the outlet water temperature and the evaporated water show substantial

161 absolute error. Such discrepancies are further discussed below.

162   The temperature gap between MOSAT and TRANSAT 2.0 is due both to thermal loss from the saturator system to external

163 environment and to the over-saturation of the output gas stream [13].

164

165   <u>a) Thermal Loss</u>

166   The saturation tower heat loss comes primarily from two sources:

167   (i)   four coupling flanges, not insulated, Figure 4

168   (ii)   insulation shell around the tower, Figure 4

169   These heat losses were estimated to evaluate the possibility to integrate such estimation directly into the code.

170   To model these losses, we assumed a radial conduction through the tower wall and free-convection from the external bound of the

171 wall to surrounding area. The following equations were used:

$$q_{out_{flanges}} = \frac{\bar{T} - T_{\infty}}{R_t} \tag{16}$$

172

173 where $\bar{T}$ is the mean temperature in the tower and it is equal to

$$\bar{T} = \Sigma_{n=1}^4 \frac{T_{g_n} + T_{l_n}}{2} \Big/ 4 \tag{17}$$

174

175 where the T_n are the temperatures measured along the saturator axis, excluding tower ends, see Figure 4.

176 The total resistance, see Figure 5, R_t is considered as a series of conductive (k) and convective (c) contributions:

$$R_t = R^k + R^c \tag{18}$$

$$R^k{}_{flange} = \frac{1}{2\pi \cdot L \cdot \sigma} \cdot \ln\frac{r_{external}}{r_{internal}} \tag{19}$$

177

178 in which L is the total thickness of the 4 flanges along tower longitudinal axis and σ is the conductivity of the steel of the flanges.

$$R^c = \frac{1}{A_e \cdot h^c_e} + \frac{1}{A_i \cdot h^c_i} \tag{20}$$

179

180 In (19) A is the total exchange area, h^c_i is the internal convective coefficient and h^c_e is the external convective coefficient.

181 A gross estimation of the internal radial convective heat transfer was conducted, although the evaluation of the heat transfer coefficient

182 is very difficult due to the complex characteristics of the fluid (two phase, change of state). The correlations presented in [8] were

183 used. Considering the humid air phase only, the h^c varied, depending on the flow characteristics, from 4 to 7 $W/(m^2 K)$; for the liquid

184 phase only h^c varied from 65 to 100 $W/(m^2 K)$. On top of that it is reasonable to consider that a liquid film covers the whole internal

185 surface of the pipe, hence the heat exchange towards the pipe is driven by the liquid phase according to its heat transfer coefficient.

186 The mass transfer between liquid and gas phase balances the heat transferred by the liquid to the pipe. In conclusion, the convective

187 coefficient inside the pipe is assumed to be equal to the liquid convective coefficient.

188 Regarding the thermal resistance of the insulation shell, the approach is the same as for the flanges.

189 Table 4 reports the coefficients used for estimation of heat losses: the h^c_e coefficient is calculated by the simplified dimensional

190 equation (21) proposed by [8] for natural convection.

$$h = b \cdot (\Delta T)^m \cdot L^{3m-1} \tag{21}$$

191

192 where m and b are chosen as 0.25 and 1.37 respectively.

193 The thermal fluxes calculated with (16) are subtracted from the water thermal flow at the exit in order to estimate the impact

194 caused by heat losses on such a measurable parameter, see equations (22) and (23).

$$\Delta T_{flanges} = \frac{q_{out_{flanges}}}{c_{p,l} \cdot \dot{m}_l} \tag{22}$$

$$\Delta T_{insulation} = \frac{q_{out_{insulation}}}{c_{p,l} \cdot \dot{m}_l} \tag{23}$$

195

196 $c_{p,l}$ is the constant pressure specific heat of the liquid current at the outlet conditions.

197

198 b) Over- saturation

199 MOSAT project has shown a systematic over-saturation of the outlet gas stream, the absolute humidity of the air at tower top

200 being of the order of 10% greater than the saturation limit [13]. This observation is confirmed by comparison between theoretical

201 saturation and experimental data (Table 3).

202 For the estimation of the impact of the over-saturation, in terms of outlet water temperature, the following equations were used:

$$q_{os} = \left[h_l \left(T_{l_{out}} \right) - h_v \left(p_{v_{out}} \right) \right] \cdot \Delta d\dot{m}_l \tag{24}$$

$$\Delta d\dot{m}_l = d\dot{m}_{l_{MOSAT}} - d\dot{m}_{l_{TRANSAT}} \tag{25}$$

$$\Delta T_{os} = \frac{q_{os}}{c_{p,l} \cdot \dot{m}_{l_{out}}} \tag{26}$$

203

204 The ΔT calculated with equations (21), (22) and (26) are shown in Table 5, where T^* corresponds to:

$$T^* = T_{l_{out_{TRANSAT}}} + \Delta T_{flanges} + \Delta T_{insulation} + \Delta T_{os} \tag{27}$$

205

206 It is straightforward to see that the total thermal losses caused by conductive and convective heat transmission and the presence of

207 a systematic over-saturation are sufficient to explain and justify the differences between simulated and experimental water outlet

208 temperature. In conclusion, from Table 5, it can be observed that the maximum error on water outlet temperature estimation made by

209 TRANSAT 2.0 code is lower than 1.25 % in absolute value.

210 Figure 6 shows the reduction of the water outlet temperature difference between calculated and experimental data switching from

211 raw TRANSAT output values to T* corrected values.

212 Figure 7 shows the comparison between MOSAT and TRANSAT 2.0 on the water and gas temperatures evolution versus the non-

213 dimensional height of the saturator for the test case number 4. In the secondary y axis the evolution of the gas stream relative humidity

214 is reported. It is easy to notice that the air saturation is completed at about the 25% of the tower height and the largest part of the heat

215 transfer is accomplished in the same fraction of the saturator.

6. TRANSIENT ANALYSIS FEATURES

217 Even though the code has been validated only in steady- state conditions, TRANSAT 2.0 retains transient analysis capability. In

218 this respect improved numerical stability was reached due to a better estimation of gas and water mass in the elementary cells and a

219 more accurate updating of molar compositions of the air stream across following iterations.

220 A significant example of improved stability is the analysis of the time response of the model forced by a double step input

221 variation. The startup time is ignored.

222 Figure 8 shows the comparison between two simulations performed with TRANSAT 1.0 (left) and TRANSAT 2.0 (right).

223 In order to investigate the saturator response to small system disturbances, the water inlet temperature was changed through a

224 sequence of two steps: starting from a stable regime, first a +5% variation was done, and then, after new stable regime attained, a

225 second step change of -10%.

226   The difference between the two behaviours is very clear: TRANSAT 1.0 shows instability in the output gas temperature, within

227   the time range where the double step is imposed, while TRANSAT 2.0 now shows a stable trend.

7. CONCLUSIONS AND PERSPECTIVES

229   The upgrade and validation efforts towards the TRANSAT release 2.0 allow the following conclusions to be drawn:

230

231   a) This latest release of TRANSAT is able to simulate saturator on-design and off-design conditions with good accuracy on all

232   the significant parameters except the water outlet temperature and the evaporated water;

233   b) Including thermal loss estimation the error on water temperature is less than 1% (MOSAT standard deviation $\sigma = 2.832$ K

234   [13]);

235   c) The error of about 10% on water evaporated is in agreement with MOSAT project conclusions, as it showed consistently an

236   average 10% over-saturated gas flow at the saturator exit;

237   d) Enhanced numerical stability was achieved;

238   e) The computational speed is largely increased thanks to reduced number of elementary cells and increased integration time

239   step;

240   f) In all the presented test cases for validation the gas outlet stream was in saturation condition;

241   g) The validation needs to be carried out also in transient conditions, but additional experimental data are required;

242   h) A code-embedded conductive and convective thermal losses estimation needs to be implemented;

243   i) TRANSAT 2.0 is ready to be used as a steady-state design tool for pressurized saturation towers.

REFERENCES

245 [1] M. Jonsson, J. Yan, 2005, "Humidified gas turbines—a review of proposed and implemented cycles", Energy 30 (2005) 1013–

246   1078.

247 [2] T. Lindquist, M. Thern, T. Torisson, 2002, "Experimental and Theoretical Results of a Humidification Tower in an Evaporative

248   Gas Turbine Cycle Power Plant", ASME Paper 2002-GT-30127.

249 [3] H. Araki, Y. Katagiri, S. Marushima, S. Hatamiya, S. Higuchi, M. Tsukamoto, 2007, "Experimental Results of Humidification and

250   Water Recovery of The Advanced Humid Air Turbine System Pilot Plant", IGTC 2007, TS-012.

251 [4] Per M. Rosén, 2000, "Evaporative Cycles- in Theory and in Practice", Doctoral Thesis, Lund Institute of Technology, Lund,

252   Sweden.

253 [5] J. Parente, A. Traverso, A. F. Massardo, 2003, "Saturator Analysis for an Evaporative Gas Turbine Cycle", Applied Thermal

254   Engineering, Elsevier Science, 23, 1275-1293.

255 [6] R. Cevasco, J. Parente, A. Traverso, A.F. Massardo, 2004, "Off-Design and Transient Analysis of Saturators for Humid Air

256   Turbine Cycles", ASME paper GT-2004-53315.

257 [7] D. Bharathan, E. Hoo, P. D'Errico, 1992, Assessment of the Use of Direct Contact Condensers with Wet Cooling Systems for

258   Utility Steam Power Plants. 38 pp.; NICH Report No. TP-254-4514.

259   Available at http://www.osti.gov/energycitations/servlets/purl/10124218-DGQNbd/

260 [8] Perry's Chemical Engineer's Handbook (Perry R. H., Green D. – editors) , 1997, 7th edition, McGraw-Hill, New York.

261 [9] J. Parente, A. Traverso, A. Massardo, 2003, "Micro Humid Air Cycle Part A: Thermodynamic and Technical Aspects", ASME

262   paper GT-2003-38326.

263 [10]Hyland R.W., Wexler A., 1983, "Formulations for the Thermodynamic Properties of Dry Air from 173.15 to 473.15 K, and of

264   Saturated Moist Air from 173.15 K to 372.15 K, at Pressures to 5 MPa", ASHRAE Transactions, 89 No 2A, pp. 520-535.

265 [11]Hyland R.W., Wexler A., 1983, "Formulations for the Thermodynamic Properties of the Saturated Phases of H2O from 173.15 K

266   to 473.15 K", ASHRAE Transactions, 89 No 2A, pp.500-519.

267 [12]A.A. Pedemonte, A. Traverso, A.F. Massardo, 2008, "Experimental analysis of pressurised humidification tower for humid air gas

268   turbine cycles. Part A: Experimental campaign", Applied Thermal Engineering, Elsevier Science, Vol. 28, 1711–1725.

269 [13]A.A. Pedemonte, A. Traverso , A.F. Massardo, 2008, "Experimental analysis of pressurised humidification tower for humid air

270   gas turbine cycles. Part B: Correlation of experimental data", Applied Thermal Engineering, Elsevier Science, Vol. 28, 1623-1629.

271 [14]A. Traverso, A. F. Massardo, 2002, "Thermoeconomic Analysis of Mixed Gas-Steam Cycles", Applied Thermal Engineering,

272   Elsevier Science, 22, 1-21.

273 **APPENDIX A: UNCERTAINTY OF EXPERIMENTAL DATA**

274

275   *Temperature and pressure*

276   All thermocouples installed to monitor the tower body and to control the inlet temperatures are "K" type class 1. Such

277 thermocouples provide Type A uncertainty errors of ±1.5°C over the range -40°C -1000°C.

278   For ease of construction the inlet air temperature is measured as close as possible to the saturator body. A few centimeters gap

279 between the point of measure and the saturator remained, thus leading to a displacement error in the inlet temperature. Such an error

280 was estimated as being less than 2°C, which was considered acceptable.

281   Piezoresistive absolute and differential pressure transducers were used providing Type A uncertainty of ±2% from 0°C to 50°C

282 and ±4% from -20°C to 80°C.

283

284   *Outlet air humidity – Water consumption measurement*

285   One of the most challenging problems of saturation towers is the accurate measurement of humidity of the air at the tower outlet.

286 In fact, the difference in water mass flow between inlet and outlet may be small enough to severely affect the precision of the resulting

287 consumption (each water flow meter comes with an error of ±1%, thus the error in water consumption may be in excess of ±30%,

288 depending on the operating conditions). According to the procedure employed in [2], it was decided not to use the in-line water flow

289 measurements. Water consumption was estimated by averaging over a certain period of time the feed water which had to be supplied

290 to the system in order to restore the level to the bottom of the tower. In fact, the approach consists in estimating the time that a known

291 amount of water takes to flow out of the saturator with the humid air, while the operating regime of the saturator remains unchanged.

292 This system provides a value that is a mean over a time period, but it improves measurement accuracy. The on-line water flow

293 measurements were employed to only to estimate the L/G ratio, i.e. the ratio between the water mass flow and dry air mass flow at

294 saturator inlets (top and bottom, respectively), which is an important operating parameter for the saturator.

295   Since the outlet humidity was measured by calculating the time for the saturator to consume a certain amount of water, the

296 resulting precision was relatively high, being about ±0.5%.

297

LIST OF FIGURES AND TABLES

Figure 1- TRANSAT 2.0 main interface mass

Figure 2 - Saturator elementary cell

Figure 3 - Structured internal packing

Figure 4 - Two modules of MOSAT saturation tower: 1.insulated pipe, 2.thermocouples, 3.uninsulated flanges

Figure 5- Series of thermal resistances for the evaluation of heat losses

Figure 6 - Reduction of Liquid Temperature error

Figure 7 - Gas relative Humidity and Temperatures evolution vs tower height (MOSAT-TRANSAT comparison)

Figure 8 – Comparison between TRANSAT 1.0 (left) and TRANSAT 2.0 (right): response to double step (+5%, -10%) of inlet water temperature

Table 1 - Experimental input data for TRANSAT 2.0 validation

Table 2 - Comparison between MOSAT data and TRANSAT 2.0 output results
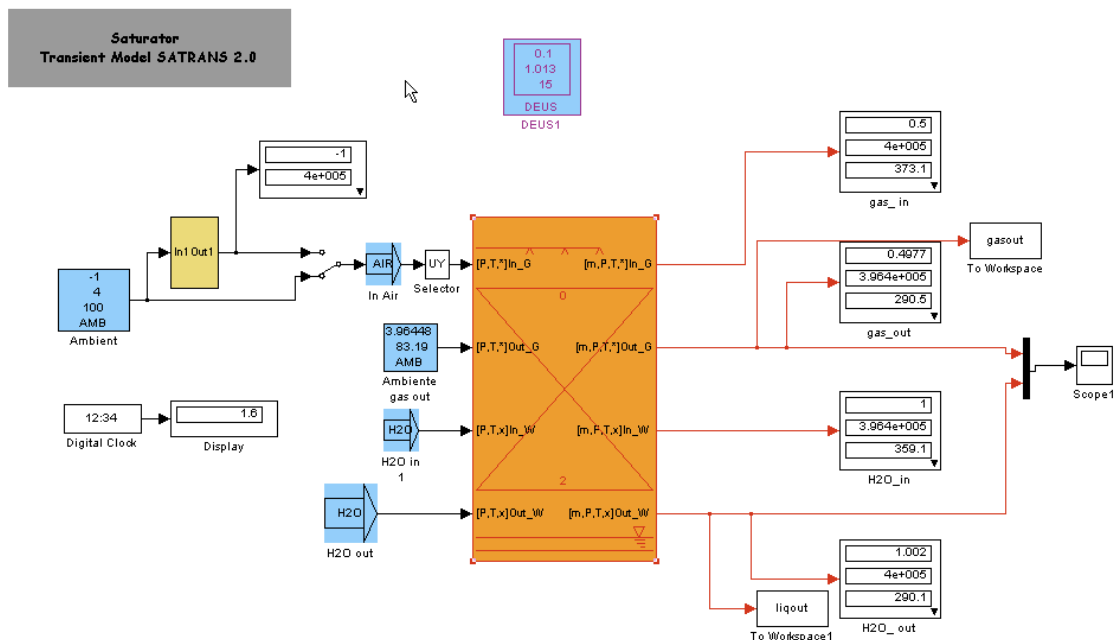
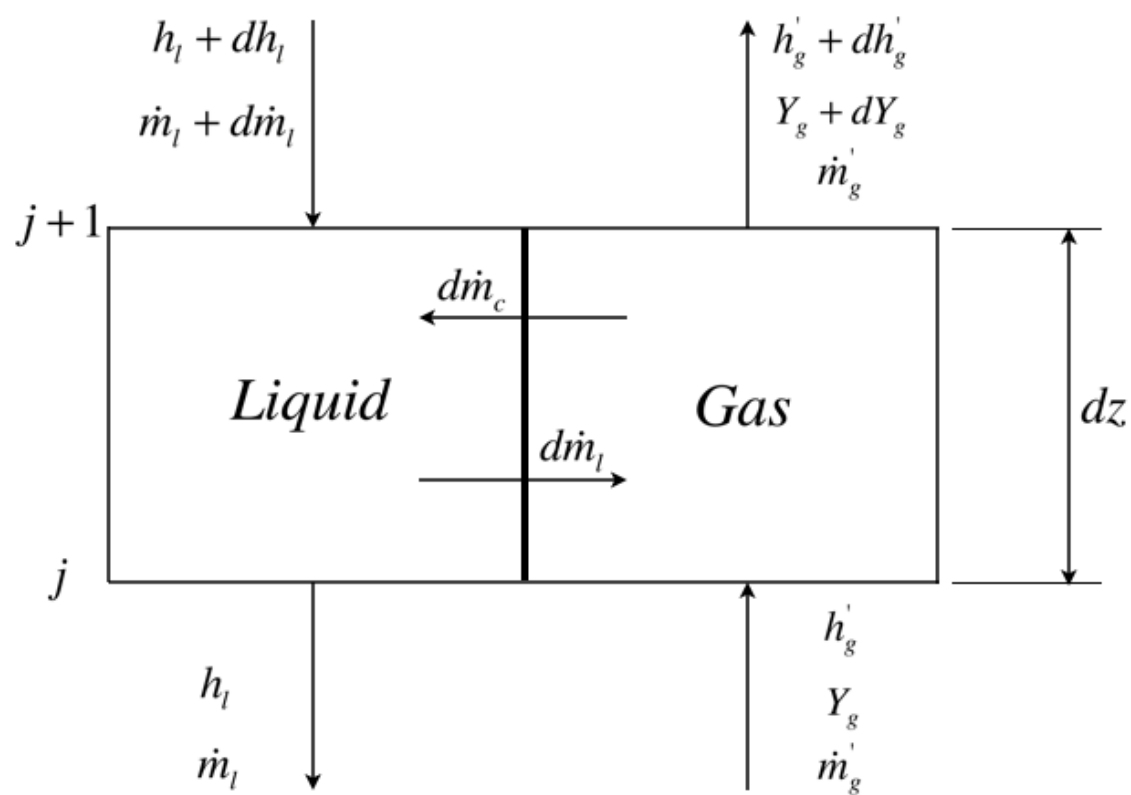**Table 3 -MOSAT - TRANSAT 2.0 absolute differences**

Table 4 - Values used for estimation of thermal loss

Table 5 - Comparison between MOSAT and TRANSAT 2.0 water outlet temperature including thermal losses
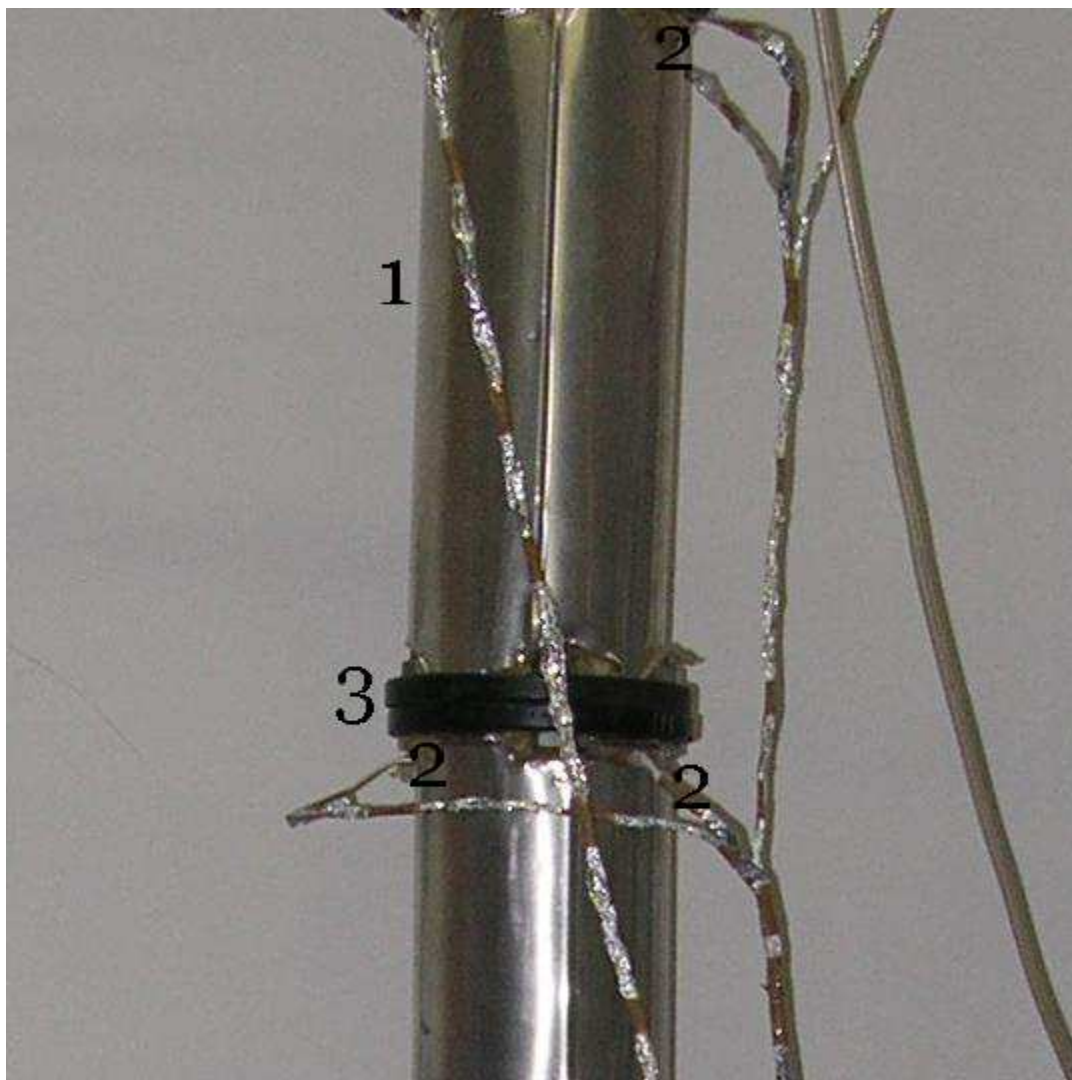
- TRANSAT is able to simulate saturator behavior with good accuracy;

- Including thermal loss estimation the error on water temperature is less than 1% ;

- Enhanced numerical stability was achieved;

- The computational speed is largely increased without loss of accuracy;

- TRANSAT 2.0 is ready to be used as a design tool for pressurized saturation towers.

**Saturator
Transient Model SATRANS 2.0**

DEUS1

-1
4e+005

In1 Out1

-1
4
100
AMB
Ambient

In Air

Selector

UY

gas_in
0.5
4e+005
373.1

gasout
To Workspace

gas_out
0.4977
3.964e+005
290.5

Ambiente
gas out

12:34
Digital Clock

1.6
Display

H2O in
1

H2O out
H2O

H2O_in
1
3.964e+005
359.1

Scope1

liqout
To Workspace1

H2O_out
1.002
4e+005
290.1

$h_l + dh_l$

$\dot{m}_l + d\dot{m}_l$

$h_g^{'} + dh_g^{'}$

$Y_g + dY_g$

$\dot{m}_g^{'}$

$j+1$

$d\dot{m}_c$

Liquid

$d\dot{m}_l$

Gas

dz

j

h_l

$\dot{m}_l$

$h_g^{'}$

Y_g

$\dot{m}_g^{'}$

$Insulation$

R_{int}^C $\overline{T}$ R^k R_{ext}^C T_∞

test n°	p (bar)	T_{gin} (° C)	T_{lin} (° C)	m_{gin} (g/s)	m_{lin} (g/s)	L/G
1	3	101	76	10	10	1
2	4	300	129	10	10	1
3	4	200	129	10	10	1
4	4	100	86	5	10	2
5	4	200	86	10	5	0.5
6	5	200	135	10	10	1

n°	MOSAT			TRANSAT 2.0		
	T_g out	T_l out	dm_l (g/s)	T_g out	T_l out	dm_l (g/s)
1	64.0	46.4	0.62	63.9	51.0	0.58
2	92.9	79.6	1.85	92.8	88.5	1.67
3	92.6	68.6	1.99	92.0	77.1	1.80
4	83.2	65.0	0.50	82.3	68.1	0.46
5	76.9	68.2	0.86	76.6	76.3	0.78
6	99.7	73.2	2.09	99.5	78.0	1.90

	MOSAT - TRANSAT 2.0			
n°	ΔT_g out	ΔT_l out	dm_l	% error dm_l
1	0.2	-4.6	0.04	6.5%
2	0.1	-8.9	0.18	9.7%
3	0.6	-8.5	0.19	9.7%
4	0.8	-3.1	0.04	8.4%
5	0.2	-8.3	0.08	9.1%
6	0.1	-4.8	0.19	9.1%

	Flanges	Insulation
T_∞	25	25
r internal	0.04 m	0.04 m
r external	0.12 m	0.10 m
L	0.12 m	1.48 m
k	10 W/m•K	0.2 W/m•K
h_e	4-6 W/m^{2}K	4-6 W/m^{2}K
h_i	65-100 W/m^{2}K	65-100 W/m^{2}K

n°	$\Delta T_{Flanges}$	ΔT_{Ins}	ΔT_{os}	ΔT_{total}	T_l*	error on T_l [°C]	enthalpy balance %
1	2.9	0.5	1.2	4.6	46.4	0.0	0.32
2	5.1	0.9	1.9	7.9	80.6	1.0	0.21
3	4.9	1.0	1.8	7.8	69.2	0.8	0.37
4	1.5	0.4	1.0	2.8	65.2	0.3	0.26
5	4.8	0.9	1.8	7.6	68.7	0.8	0.05
6	2.3	0.1	1.6	4.0	74.0	0.8	0.12